J. Appl. Comput. Mech., 5(1) (2019) 77-90
DOI: 10.22055/JACM.2018.25692.1287

ISSN: 2383-4536
jacm.scu.ac.ir

M&MoCS

Shahid Chamran University of Ahvaz

Journal of Applied and Computational Mechanics

Research Paper

# Study on Free Vibration and Wave Power Reflection in Functionally Graded Rectangular Plates using Wave Propagation Approach

**A. Zargaripoor, A. Daneshmehr, M. Nikkhah Bahrami**

School of Mechanical Engineering, College of Engineering, University of Tehran, Tehran, Iran.

Received April 29 2018; Revised May 13 2018; Accepted for publication May 22 2018.
Corresponding author: A. Daneshmehr daneshmehr@ut.ac.ir.


**Abstract.** In this paper, the wave propagation approach is presented to analyze the vibration and wave power reflection in FG rectangular plates based on the first order shear deformation plate theory. The wave propagation is one of the useful methods for analyzing the vibration of structures. This method gives the reflection and propagation matrices that are valuable for the analysis of mechanical energy transmission in devices. It is assumed that the plate has two opposite edges simply supported while the other two edges may be simply supported or clamped. It is the first time that the wave propagation method is used for functionally graded plates. In this study, firstly, the matrices of reflection and propagation are derived. Second, these matrices are combined to provide an exact method for obtaining the natural frequencies. It is observed that the obtained results of the wave propagation method are in a good agreement with the obtained values in literature. At the end, the behavior of reflection coefficients for FG plates are studied for the first time.

**Keywords**: Rectangular FG plate; Propagation matrix; Reflection matrix; Vibration analysis; FSDT.

## 1. Introduction

As powerful engines, turbines, reactors, and other machines have been developed in recent years in aerospace industries, the need for materials with high thermal and mechanical resistance has been identified. The gradual change in structure and properties has caused the application of such materials to spread, particularly in cases where different properties are needed in different regions. A common type of FGM includes a continuous combination of a ceramic and a metal. The change from pure metal to pure ceramic is incremental and continuous such that one surface is made of pure ceramic and the other of pure metal. The mechanical properties also change continuously through the thickness based on the compound type.

The free vibrations of functionally graded materials have been studied widely in recent years. Zhao et al. [1] presented the free vibration analysis of metal and ceramic functionally graded plates that uses the element-free kp-Ritz method. Meiche et al. [2] presented a new hyperbolic shear deformation theory by taking into account the transverse shear deformation effects for the buckling and free vibration analysis of thick functionally graded sandwich plates. Hosseini-Hashemi et al. [3] presented an analytical solution for free vibration analysis of moderately thick rectangular plates which are composed of functionally graded materials and supported by either Winkler or Pasternak elastic foundations. Akbas [4] presented the free vibration analysis of an edge cracked functionally graded cantilever beam. Thai and Vo [5] developed a new sinusoidal shear deformation theory for bending, buckling, and vibration of functionally graded plates. Mahi and Tounsi [6] presented a new hyperbolic shear deformation theory applicable to bending and free vibration analysis of isotropic, functionally graded, sandwich, and laminated composite plates. Akbas [7] presented the free vibration and bending of functionally graded beams resting on elastic foundation. Bennoun et al. [8] developed a new five-variable plate theory for the free vibration analysis of functionally graded sandwich plates. Zhang et al. [9] employed the first order shear deformation theory to account for the effect of transverse shear

Published online December 14 2018

deformation of the plates and used the element-free IMLS-Ritz method for numerical computation. Khorshidi et al. [10] investigated the free vibration analysis of the functionally graded rectangular nanoplates. Bellifa et al. [11] developed a new first-order shear deformation theory for bending and dynamic behaviors of functionally graded plates. Pradhan and Chakraverty [12] investigated the free vibration of functionally graded elliptic plates subjected to various classical boundary conditions. Houari et al. [13] developed a new simple higher-order shear deformation theory for bending and free vibration analysis of functionally graded plates. Bounouara et al. [14] presented a zeroth-order shear deformation theory for the free vibration analysis of functionally graded nanoscale plates resting on the elastic foundation. Abdelbari [15] presented a simple hyperbolic shear deformation theory for the analysis of functionally graded plates resting on the elastic foundation. Seref Doguscan [16] presented the free vibration and the static bending of a simply supported functionally graded plate with the porosity effect. Bessaim et al. [17] studied the mechanical buckling response of refined hyperbolic shear deformable functionally graded nanobeams embedded in an elastic foundation based on the refined hyperbolic shear deformation theory. Fouda et al. [18] presented the effect of porosity on mechanical behaviors of a power distribution functionally graded beam. Song et al. [19] investigated the free and forced vibration characteristics of functionally graded multilayer grapheme nanoplatelet (GPL)/polymer composite plates within the framework of the first-order shear deformation plate theory. Akbas [20] presented the stability analysis of a non-homogeneous plate with porosity effect. Moreover, Akbas [21] investigated the free vibration analysis of edge cracked cantilever microscale beams composed of functionally graded material based on the modified couple stress theory. In other work. Akbas [22] presented forced vibration responses of functionally graded nanobeams for the modified couple stress theory with damping effect. In addition, Akbas [23] investigated the thermal effects on the free vibration of functionally graded porous deep beams. Recently, Akbas [24] investigated the forced vibration analysis of functionally graded porous deep beams under the dynamic load.

Even though there are some classical analytical and exact solutions of the plate theory, in these methods, the natural frequencies are obtained by applying the boundary conditions to the general solution of the differential equation. There is an alternative approach called the wave propagation method which considers vibrations as propagating waves traveling in the structures.

Mace [25] expressed the vibrational behavior of beam systems in terms of waves of both propagating and near field types. Mei and Mace [26] presented wave reflection, transmission, and propagation in Timoshenko beams together with the wave analysis of vibrations in Timoshenko beam structures. Nikkhah Bahrami et al. [27] presented the modified wave approach for calculation of natural frequencies and mode shapes in arbitrary non-uniform beams. Bahrami et al. [28] analyzed the free vibration of annular circular and sectorial membranes using the wave propagation approach. In other work, Bahrami and Teimourian [29] combined the wave propagation approach with the nonlocal elasticity theory to analyze the buckling and free vibration of Euler-Bernoulli nanobeams. Ilkhani et al. [30] used the wave propagation approach to analyze the free vibrations analysis of thin rectangular macro- and nano-plates. Bahrami and Teimourian [31] presented the wave propagation approach for analyzing the free vibration and wave reflection in carbon nanotubes. Moreover, they presented the wave propagation approach for free vibration analysis of nan-uniform annular and circular membranes [32]. Recently, Bahrami and Teimourian [33] presented the wave propagation approach for free vibration analysis of non-uniform rectangular membranes. Moreover, Bahrami and Teimourian [34] developed the wave propagation technique for analyzing the wave power reflection in circular annular nanoplates. In another work, Bahrami [35] utilized the wave propagation method and the differential constitutive law consequent to the Eringen strain-driven integral nonlocal elasticity model to analyze the free vibration, wave power transmission, and reflection in multi-cracked nanorods. In addition, Bahrami [36] utilized the wave propagation method and the nonlocal elasticity theory to analyze the vibration, wave power transmission, and reflection in multi-cracked Euler-Bernoulli nanobeams. Akbas [37] presented responses of an edge circular cantilever beam under the effect of an impact force. Besides, Akbas [38] investigated the effect of material-temperature dependent on the wave propagation of a cantilever beam composed of functionally graded material under the effect of an impact force. In another work, Akbas [39] studied the wave propagation in an edge cracked cantilever beam composed of functionally graded material under the effect of an impact force.

According to the above-mentioned literature review, the wave propagation method for functionally graded plates has not been addressed. In addition, for the first time the effect of power law index on the wave power reflection is studied. In this study, first, the matrices of propagation and reflection are derived and next, by combining them, the characteristic equation of the plate is obtained.

## 2. Modeling and Formulation

### 2.1 Geometrical configuration

In Figure 1, a functionally graded rectangular plate of length, width, and height is shown. Cartesian coordinates is considered.

### 2.2 Material properties

The functionally graded plate consists of two metal and ceramic parts which are integrated in such a way that material properties are continuously and gradually changed along with the plate thickness from purely metal properties in the bottom surface of plate $(z=-\frac{h}{2})$ to purely ceramic properties in the top of the plate $(z=+\frac{h}{2})$. Assuming that the distribution of the material properties through thickness follows the power law, the following equation could be written.

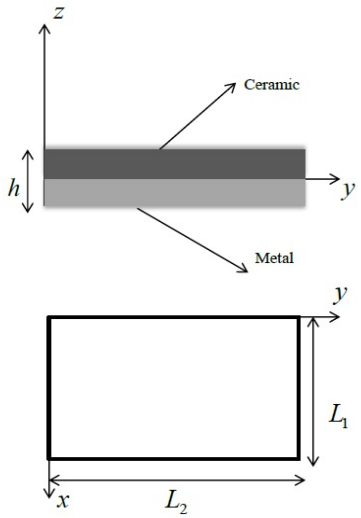


**Fig 1.** Geometry of functionally graded rectangular plate

$$P = P_m V_m + P_c V_c \tag{1}$$

where $P_m$ and $P_c$ show metal and ceramic properties and $V_m$ and $V_c$ show the volume fraction of the metal and ceramic parts in the bottom and top surfaces of the plate, respectively. By using the power distribution law, the volume fraction of the ceramic part is noted for each point of plate thickness in Eqs. (2) and (3). [40]

$$V_c = (\frac{z}{h} + \frac{1}{2})^n \tag{2}$$

$$V_m + V_c = 1 \tag{3}$$

Where $n$ indicates the power law index of ceramic and the distribution of ceramic part is noted along with the plate. Therefore, according to the above-mentioned equation, the properties of the graded materials is a function of $E$, Young modulus, and unit mass of volume $\rho$ along with the plate thickness as shown in the following equations.

$$E(z) = (E_c - E_m)V_c + E_m \tag{4}$$

$$\rho(z) = (\rho_c - \rho_m)V_c + \rho_m \tag{5}$$

### 2.3 Governing Equations of motion

The displacement components in Mindlin plate are assumed to be given as

$$u = -z\varphi_x(x, y, t) \tag{6a}$$

$$v = -z\varphi_y(x, y, t) \tag{6b}$$

$$w = \varphi_z(x, y, t) \tag{6c}$$

where $u, v$, and $w$ are the mid-plane displacements and $\varphi_x$ and $\varphi_y$ show normal rotation perpendicular to the middle of the plate around $y$ and $x$ axes, respectively. $\varphi_z$ is the transverse displacement and $t$ is the time variable. The strain equation could be written by using the above-mentioned displacement fields as follows:

$$\varepsilon_{xx} = -z\,\varphi_{x,x} \tag{7a}$$

$$\varepsilon_{yy} = -z\,\varphi_{y,y} \tag{7b}$$

$$\varepsilon_{zz} = 0 \tag{7c}$$

$$\gamma_{xy} = -\frac{z}{2}\left(\varphi_{x,y} + \varphi_{y,x}\right) \tag{7d}$$

$$\gamma_{xz} = -\frac{1}{2}\left(\varphi_x - \varphi_{z,x}\right) \tag{7e}$$

$$\gamma_{yz} = -\frac{1}{2}\left(\varphi_y - \varphi_{z,y}\right) \tag{7f}$$

Therefore, the stress-strain relations could be defined as follows:

$$\sigma_{xx} = \frac{E(z)}{1-\nu^2}(\varepsilon_{xx} + \nu\varepsilon_{yy}) \tag{8a}$$

$$\sigma_{yy} = \frac{E(z)}{1-\nu^2}(\varepsilon_{yy} + \nu\varepsilon_{xx}) \tag{8b}$$

$$\sigma_{zz} = 0 \tag{8c}$$

$$\tau_{xy} = G(z)\gamma_{xy} \tag{8d}$$

$$\tau_{xz} = G(z)\gamma_{xz} \tag{8e}$$

$$\tau_{yz} = G(z)\gamma_{yz} \tag{8f}$$

The stress resultants in the elastic plate are defined as follows:

$$M_{xx} = -Ah^3(\varphi_{x,x} + \nu\varphi_{y,y}) \tag{9a}$$

$$M_{yy} = -Ah^3(\varphi_{y,y} + \nu\varphi_{x,x}) \tag{9b}$$

$$M_{xy} = -\frac{(1-\nu^2)}{2}Ah^3(\varphi_{x,y} + \nu\varphi_{y,x}) \tag{9c}$$

$$Q_x = -k^2hB(\varphi_x - \varphi_{z,x}) \tag{9d}$$

$$Q_y = -k^2hB(\varphi_y - \varphi_{z,y}) \tag{9e}$$

where

$$A = \frac{1}{(1-\nu^2)}\left[\frac{n(8+3n+n^2)E_m + 3(2+n+n^2)E_c}{12(1+n)(2+n)(3+n)}\right] \tag{10a}$$

$$B = \frac{1}{2(1+\nu)}\frac{E_c + nE_m}{1+n} \tag{10b}$$

and $k^2$ is the shear correction factor. The governing differential equations of motion for the mindlin plate can be found as follows:

$$M_{xx,x} + M_{xy,y} - Q_x = -\frac{1}{12}Ch^3\ddot{\varphi}_x \tag{11a}$$

$$M_{xy,x} + M_{yy,y} - Q_y = -\frac{1}{12}Ch^3\ddot{\varphi}_y \tag{11b}$$

$$Q_{x,x} + Q_{y,y} - P = Dh^3\ddot{\varphi}_z \tag{11c}$$

where

$$C = \left[\frac{n(8+3n+n^2)\rho_m + 3(2+n+n^2)\rho_c}{(1+n)(2+n)(3+n)}\right] \tag{12a}$$

$$D = \frac{\rho_c + n\rho_m}{1+n} \tag{12b}$$

where dot-overscript denotes the derivation with respect to $t$. For generality and convenience, the following dimensionless terms are defined.

$$X = \frac{x}{L_1},\ Y = \frac{y}{L_2},\ \tau = \frac{h}{L_1},\ \eta = \frac{L_1}{L_2},\ \beta = \omega a^2\sqrt{\frac{C}{Ah^2}} \tag{13}$$

where $\tau$, $\eta$, and $\beta$ are thickness to length ratio, aspect ratio, and Eigen frequency parameter. The non-dimensional equations of motion based on the Mindlin plate theory by using dimensionless terms are as follows [3]:

$$\bar{\varphi}_{x,xx}+\eta^2\bar{\varphi}_{x,yy}+\frac{\nu_2}{\nu_1}(\bar{\varphi}_{x,xx}+\eta\bar{\varphi}_{y,xy})-\frac{k^2B}{A\tau^2\nu_1}(\bar{\varphi}_x-\bar{\varphi}_{z,x})+\frac{\beta^2\tau^2}{12\nu_1}\bar{\varphi}_x=0 \tag{14a}$$

$$\bar{\varphi}_{y,xx}+\eta^2\bar{\varphi}_{y,yy}+\frac{\nu_2}{\nu_1}\eta(\bar{\varphi}_{x,xy}+\eta\bar{\varphi}_{y,yy})-\frac{k^2B}{A\tau^2\nu_1}(\bar{\varphi}_y-\bar{\varphi}_{z,y})+\frac{\beta^2\tau^2}{12\nu_1}\bar{\varphi}_y=0 \tag{14b}$$

$$\bar{\varphi}_{z,xx}+\eta^2\bar{\varphi}_{z,yy}-(\bar{\varphi}_{x,x}+\eta\bar{\varphi}_{y,y})-\frac{DA\beta^2\tau^2}{BCk^2}\bar{\varphi}_z=0 \tag{14c}$$

where $\nu_1=\frac{1-\nu}{2}$ and $\nu_1=\frac{1+\nu}{2}$. $\bar{\varphi}_x$, $\bar{\varphi}_y$, and $\bar{\varphi}_z$ are the dimensionless rotational and transverse displacements which are defined as follows:

$$\bar{\varphi}_x(X,Y,t)=\varphi_x(x,y)e^{-i\omega t} \tag{15a}$$

$$\bar{\varphi}_y(X,Y,t)=\varphi_y(x,y)e^{-i\omega t} \tag{15b}$$

$$\bar{\varphi}_z(X,Y,t)=\frac{\varphi_z(x,y)e^{-i\omega t}}{L_1} \tag{15c}$$

where $\omega$ is the natural frequency of the plate.

## 3. Solving by the wave propagation method

By defining the non-dimensional functions $\bar{\varphi}_x$, $\bar{\varphi}_y$, and $\bar{\varphi}_z$ in the form of the dimensionless functions of potential $W_1$, $W_2$, $W_3$, and $W_4$, the governing equations can be obtained [3] as

$$\bar{\varphi}_x=f_1W_{x,x}+f_2W_{y,x}-\eta W_{z,y} \tag{16a}$$

$$\bar{\varphi}_y=f_1\eta W_{x,y}+f_2\eta W_{y,y}-W_{z,x} \tag{16b}$$

$$\bar{\varphi}_z=W_x+W_y \tag{16c}$$

where

$$f_i=\frac{DA\tau^2\beta^2}{BCk^2\alpha_i^2}\quad(i=1,2) \tag{17}$$

If the equations of motion are rewritten, the differential equations will be decoupled for these functions as

$$W_{x,xx}+\eta^2W_{x,yy}=-\alpha_1^2W_x \tag{18a}$$

$$W_{y,xx}+\eta^2W_{y,yy}=-\alpha_2^2W_y \tag{18b}$$

$$W_{z,xx}+\eta^2W_{z,yy}=-\alpha_3^2W_z \tag{18c}$$

In which $\alpha_1^2,\alpha_2^2$, and $\alpha_3^2$ are defined as follows:

$$\alpha_1^2=\frac{\beta^2(12\frac{D}{C}+\tau^2\frac{Bk^2}{A\tau^2})}{24\frac{Bk^2}{A\tau^2}}+\frac{1}{24}\sqrt{\frac{-48\frac{Bk^2}{A\tau^2}(\beta^2\tau^2-12\frac{Bk^2}{A\tau^2})(\frac{D\beta^2}{C})+(\beta^2(12\frac{D}{C}+\tau^2\frac{Bk^2}{A\tau^2}))^2}{(\frac{Bk^2}{A\tau^2})^2}} \tag{19a}$$

$$\alpha_1^2=\frac{\beta^2(12\frac{D}{C}+\tau^2\frac{Bk^2}{A\tau^2})}{24\frac{Bk^2}{A\tau^2}}-\frac{1}{24}\sqrt{\frac{-48\frac{Bk^2}{A\tau^2}(\beta^2\tau^2-12\frac{Bk^2}{A\tau^2})(\frac{D\beta^2}{C})+(\beta^2(12\frac{D}{C}+\tau^2\frac{Bk^2}{A\tau^2}))^2}{(\frac{Bk^2}{A\tau^2})^2}} \tag{19b}$$

$$\alpha_1^2=\frac{Bk^2}{\nu_1A\tau^2}-\frac{\beta^2\tau^2}{12\nu_1} \tag{19c}$$

By considering the simply support conditions in the corners $X_1=0$ and $X_1=1$ and using the method of separation of variables, an answer set is obtained for equations (18) as

$$W_1 = \left[C_1 \sin\left(\mu_1 Y\right) + C_2 \cos\left(\mu_1 Y\right)\right] \sin\left(m\pi X\right) \tag{20a}$$

$$W_2 = \left[C_3 \sinh\left(\mu_2 Y\right) + C_4 \cosh\left(\mu_2 Y\right)\right] \sin\left(m\pi X\right) \tag{20b}$$

$$W_3 = \left[C_5 \sinh\left(\mu_3 Y\right) + C_6 \cosh\left(\mu_3 Y\right)\right] \cos\left(m\pi X\right) \tag{20c}$$

where

$$\alpha_1^2 = \eta^2 \mu_1^2 + (m\pi)^2 \quad \alpha_2^2 = -\eta^2 \mu_2^2 + (m\pi)^2 \quad \alpha_3^2 = -\eta^2 \mu_3^2 + (m\pi)^2 \tag{21}$$

Based on the first-order shear theory, the boundary conditions for two parallel corners (for example $X = 0$ and $X = 1$) are as follows:

$$\text{Simply supported:} \quad M_{yy} = \overline{\varphi_x} = \overline{\varphi_z} = 0 \tag{22}$$

$$\text{Clamped:} \quad \overline{\varphi_x} = \overline{\varphi_y} = \overline{\varphi_z} = 0 \tag{23}$$

By replacing the formulas $W_i$ in equations related to the potential function and considering the following equations, $\overline{\varphi_i}$ could be found as

$$\sin(\theta) = \frac{e^{i\theta} - e^{-i\theta}}{2i}; \cos(\theta) = \frac{e^{i\theta} + e^{-i\theta}}{2}; \ \sinh(\theta) = \frac{e^{\theta} - e^{-\theta}}{2}; \cosh(\theta) = \frac{e^{\theta} + e^{-\theta}}{2} \tag{24}$$

which yields

$$\begin{aligned} \overline{\varphi_x} = [&C_1' f_1 m\pi e^{i\mu_1 Y} + C_2' f_1 m\pi e^{-i\mu_1 Y} + C_3' f_2 m\pi e^{\mu_2 Y} + C_4' f_2 m\pi e^{-\mu_2 Y} \\ &+ C_5' \eta\mu_3 e^{\mu_3 Y} + C_6' \eta\mu_3 e^{-\mu_3 Y}) \cos(m\pi X_1) \end{aligned} \tag{25a}$$

$$\begin{aligned} \overline{\varphi_y} = [&C_1'' f_1 \eta\mu_1 e^{i\mu_1 Y} + C_2'' f_1 \eta\mu_1 e^{-i\mu_1 Y} + C_3'' f_2 \eta\mu_2 e^{\mu_2 Y} + C_4'' f_2 \eta\mu_2 e^{-\mu_2 Y} \\ &+ C_5'' m\pi_3 e^{\mu_3 Y} + C_6'' m\pi e^{-\mu_3 Y}] \sin(m\pi X_1) \end{aligned} \tag{25b}$$

$$\overline{\varphi_z} = [C_1''' e^{i\mu_1 Y} + C_2''' e^{-i\mu_1 Y} + C_3''' e^{\mu_2 Y} + C_4''' e^{-\mu_2 Y}] \sin(m\pi X_1) \tag{25c}$$

in which

$$C_1' = \frac{-iC_1 + C_2}{2}; \ C_2' = \frac{iC_1 + C_2}{2}; \ C_3' = \frac{C_3 + C_4}{2} \tag{26a}$$

$$C_4' = \frac{C_4 - C_3}{2}; \ C_5' = \frac{-C_6 - C_5}{2}; \ C_6' = \frac{-C_5 + C_6}{2} \tag{26b}$$

Therefore, $C_i''$ and $C_i'''$ can be written based on $C_i'$ as

$$C_1' = -iC_1'' = C_1''' \ ; C_2' = iC_2'' = C_2'''; \ C_3' = C_3'' = C_3''' \tag{27a}$$

$$C_4' = -C_4'' = C_4'''; \ C_5' = C_5'' = A_5'''; \ C_6' = -C_6'' \tag{27b}$$

Finally, it yields

$$\overline{\varphi_x} = \begin{bmatrix} C_1' f_1 m\pi e^{i\mu_1 Y} + C_2' f_1 m\pi e^{-i\mu_1 Y} + C_3' f_2 m\pi e^{\mu_2 Y} + C_4' f_2 m\pi e^{-\mu_2 Y} \\ C_5' \mu_3 \eta e^{\mu_3 Y} + C_6' \mu_3 \eta e^{-\mu_3 Y} \end{bmatrix} \cos\left(m\pi X_1\right) \tag{28a}$$

$$\overline{\varphi_y} = \begin{bmatrix} C_1' i f_1 \mu_1 e^{i\mu_1 Y} - C_2' i f_1 \mu_1 e^{-i\mu_1 Y} + C_3' f_2 \mu_2 \eta e^{\mu_2 Y} - C_4' f_2 \mu_2 \eta e^{-\mu_2 Y} \\ + C_5' m\pi e^{\mu_3 Y} - C_6' m\pi e^{-\mu_3 Y} \end{bmatrix} \sin\left(m\pi X_1\right) \tag{28b}$$

$$\overline{w} = \left[C_1' e^{i\mu_1 Y} + C_2' e^{-i\mu_1 Y} + C_3' e^{\mu_2 Y} + C_4' e^{-\mu_2 Y}\right] \sin\left(m\pi X_1\right) \tag{28c}$$

Sentences with even indexes display a wave in the positive direction of the dimensionless $Y$ axis and sentences with odd indexes display a wave in the negative direction of the $Y$ axis. Therefore, it can be written as

$$a^+(x) = \begin{Bmatrix} C_2' e^{-i\mu_1 Y} \\ C_4' e^{-\mu_2 Y} \\ C_6' e^{-\mu_3 Y} \end{Bmatrix}; \quad a^-(x) = \begin{Bmatrix} C_1' e^{i\mu_1 Y} \\ C_3' e^{\mu_2 Y} \\ C_5' e^{\mu_3 Y} \end{Bmatrix} \tag{29}$$

## 4. Propagation Matrix

Figure 2 shows two points on the plate at distance $Y^0$ apart in $Y$ direction where Positive- and negative-going waves propagate from one point to another. By using Eqs. (29), they are related by

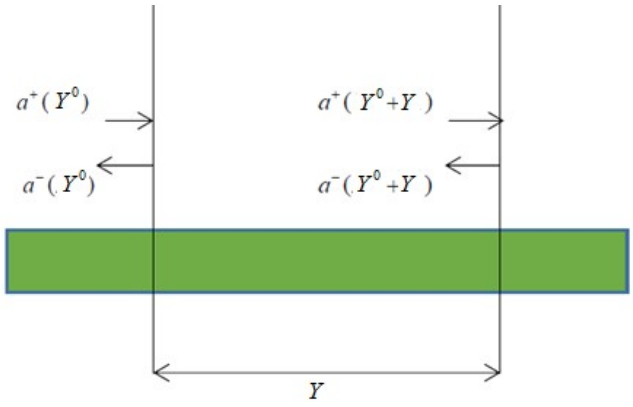


**Fig. 2.** Positive and negative going propagating waves in FG Mindlin plate

$$a^+\left(Y+Y^0\right)=F^+a^+\left(Y^0\right),\ \ a^-\left(Y^0\right)=F^-a^-\left(Y+Y^0\right) \tag{30}$$

where $F^+$ and $F^-$ are the propagation matrix in the positive and negative directions, respectively. Replacing Eq. (29) in Eq. (30) yields

$$F^+=F^-=\begin{bmatrix} e^{-i\mu_1 Y} & 0 & 0 \\ 0 & e^{-\mu_2 Y} & 0 \\ 0 & 0 & e^{-\mu_3 Y} \end{bmatrix} \tag{31}$$

The propagation functions in the positive and negative directions are equal to each other and they are called $F$.

## 5. Reflection Matrix

When the propagated waves in the plate are collided to the boundaries, they are reflected and this action obviously presents that as long as the plate is vibrating, positive and negative waves are propagating in the environment. The equation of positive and negative travelling waves with the reflection matrix $r$ is provided as

$$a^-=ra^+ \tag{32}$$

For the simply supported and clamped boundary condition, the reflection of the propagated waves in the plate is expressed.

### 5.1 Reflection matrix for the simply support boundary condition

The conditions for the simply supported boundary are as follows:

$$M_{yy}=\overline{\varphi_x}=\overline{\varphi_z}=0 \tag{33}$$

The incoming wave to this boundary is called $a^+$ and the reflected wave from the boundary is called $a^-$.

$$\begin{aligned} M_{yy}=&\left[-f_1\mu_1^2\eta^2-f_1(m\pi)^2\nu\right]a_1^-+\left[-f_1\mu_1^2\eta^2-f_1(m\pi)^2\nu\right]a_1^+ \\ &+\left[f_2\mu_2^2\eta^2-f_2(m\pi)^2\nu\right]a_2^-+\left[f_2\mu_2^2\eta^2-f_2(m\pi)^2\nu\right]a_2^+ \\ &+\left[m\pi\eta\mu_3-\eta\mu m\pi\nu\right]a_3^-+\left[m\pi\eta\mu_3-\eta\mu m\pi\nu\right]a_3^+ \end{aligned} \tag{34a}$$

$$\overline{\varphi_x}=\left[f_1m\pi a_1^-+f_1m\pi a_1^++f_2m\pi a_2^-+f_2m\pi a_2^++\eta\mu_3a_3^-+\eta\mu_3a_3^+\right]=0 \tag{34b}$$

$$\overline{\varphi_z}=\left[a_1^-+a_1^++a_2^-+a_2^+\right]=0 \tag{34c}$$

The reflection matrix can be obtained by writing it in the form of matrix. For the simply supported mode, the reflection matrix is

$$r_s=-I \tag{35}$$

### 5.2 Reflection matrix for the Clamped boundary condition

In the clamped mode, the boundary condition is as follows:

$$\overline{\varphi_x} = \overline{\varphi_y} = \overline{\varphi_z} = 0 \tag{36}$$

$$\overline{\varphi_x} = \begin{bmatrix} f_1 m\pi a_1^- + f_1 m\pi a_1^+ + f_2 m\pi a_2^- + f_2 m\pi a_2^+ \\ +\eta\mu_3 a_3^- + \eta\mu_3 a_3^+ \end{bmatrix} = 0 \tag{37a}$$

$$\overline{\varphi_y} = \begin{bmatrix} +if_1\mu_1\eta a_1^- - if_1\mu_1\eta_1 a_1^+ + f_2\mu_2\eta a_2^- - f_2\mu_2\eta a_2^+ \\ +m\pi a_3^- - m\pi a_3^+ \end{bmatrix} = 0 \tag{37b}$$

$$\overline{w} = [a_1^- + a_1^+ + a_2^- + a_2^+] = 0 \tag{37c}$$

Therefore, the reflection matrix for the clamped mode is as follows:

$$r_C = -\begin{bmatrix} f_1 m\pi & f_2 m\pi & \eta\mu_3 \\ -if_1\mu_1\eta & -f_2\mu_2\eta & -m\pi \\ 1 & 1 & 0 \end{bmatrix}^{-1} \begin{bmatrix} f_1 m\pi & f_2 m\pi & \eta\mu \\ if_1\mu_1\eta & f_2\mu_2\eta & m\pi \\ 1 & 1 & 0 \end{bmatrix} \tag{38}$$

## 6. Analyzing the free vibrations of the FG Mindlin plate

Consider the plate shown in Fig. 2. For analyzing this plate using our wave method, two wave domains for the positive travelling wave and two wave domains for the negative travelling wave in the direction of Y at two beginning and ending points are considered. These waves can be related to each other using the obtained propagation and reflection matrices.

$$b^+ = Fa^+; a^- = Fb^- \tag{39}$$

In which $F$ is the propagation matrix of the wave between two points of A and B. Moreover, using the propagation and reflection equations in the boundaries yields

$$a^+ = r_A a^-;\ b^- = r_B b^+ \tag{40}$$

In which $r_A$ and $r_B$ are the reflection matrices in the boundaries A and B, respectively. Writing equations in the form of matrix leads to

$$\begin{bmatrix} -I & r_A & 0 & 0 \\ F & 0 & -I & 0 \\ 0 & -I & 0 & F \\ 0 & 0 & r_B & -I \end{bmatrix} \begin{bmatrix} a^+ \\ a^- \\ b^+ \\ b^- \end{bmatrix} = 0 \tag{41}$$

and for having determinant answer, this matrix must be zero. By equalizing the determinant of this matrix to zero, the frequency characteristic equation of the system is obtained.

## 7. Results and Discussion

### 7.1 Frequency calculation

The values obtained from the wave propagation method and the results obtained from the research literature are compared for the validation of the results. Here, the letters S and C represent the simply supported and clamped boundary conditions. For example, in the SCSC boundary condition, the edges along $X = 0$ and $X = 1$ are simply supported boundary conditions and the edges along $Y = 0$ and $Y = 1$ are clamped boundary conditions. The values of n and m represented the vibrational modes has n and m half-wave in x and y directions, respectively. The values of material properties for FG plates are listed in Table 1.

**Table 1.** The material properties of FG plate

| Materials | Properties | | |
|---|---|---|---|
| | $E$ (Gpa) | $\rho(Kg/m^3)$ | $\nu$ |
| $Al$ | 70 | 2702 | 0.3 |
| $Al_2O_3$ | 380 | 3800 | 0.3 |

Moreover, the shear correction factor for FG plate ( $Al / Al_2O_3$ ) is as follows [3]:

$$k^2 = \frac{5}{6} + 0.750(e^{-0.025n} - e^{-2n})(10\tau - 2) - 0.640(e^{-0.060n} - e^{-n})(10\tau - 1) \tag{42}$$

The procedure of obtaining the plate frequencies is specified by the wave propagation method as shown in Fig. 3. The plot of the real and imaginary part changes of the determinants of equation (41) in terms of the dimensionless frequency for the SCSC boundary condition and assuming m = 1, $\eta = 1$, $n = 5$, and $\tau = 0.2$ is shown in Fig. 3. As shown in the figure, the intersection of the real and imaginary curves of the determinant with the zero axis represents the roots of the determinant and hence the frequency of the plate. There is another root around natural frequency in which no marked change occurs in the real and imaginary parts. This frequency root is cut off. The cut off frequency is the frequency in which the type of wave frequencies before and after it does not change.

In Table 2, the dimensionless frequencies of the wave method are compared with reference results [1] for simply supported boundary condition, $n = 0, 0.5, 1, 4, 10$ , $\eta = 1$, and $\tau = 0.05, 0.1, 0.2$ are compared and the obtained values indicate the high accuracy of the wave propagation method. In Tables 3-5, the dimensionless frequency values for different boundary conditions of SSSS, SCSS, and SCSC are listed for different values of power law index and thickness to length ratio. The values $n = 0, 0.5, 1, 2, 5, 10$, $\eta = 1$ and $\tau = 0.05, 0.1, 0.2$ are assumed.

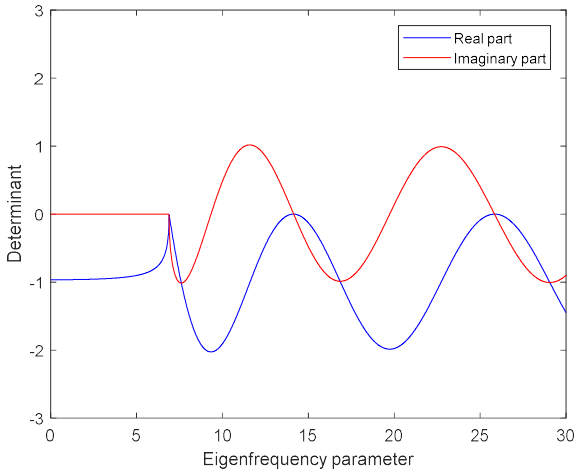


**Fig. 3.** Real and imaginary parts of determinant of Eq. (41)

**Table 2.** Dimensionless frequency $\beta^* = \omega h\sqrt{\rho_c / E_c}$ for SSSS FG square plate

| $\tau$ | Method | $n$ | | | | |
|---|---|---|---|---|---|---|
| | | 0 | 0.5 | 1 | 4 | 10 |
| 0.05 | Present [3] | 0.0148<br>0.0148 | 0.0125<br>0.0128 | 0.0113<br>0.0115 | 0.0098<br>0.0101 | 0.0094<br>0.0096 |
| 0.1 | Present [3] | 0.0577<br>0.0577 | 0.0490<br>0.0492 | 0.0442<br>0.0445 | 0.0381<br>0.0382 | 0.0364<br>0.0362 |
| 0.2 | Present [3] | 0.2114<br>0.2112 | 0.1808<br>0.1806 | 0.1652<br>0.1650 | 0.1377<br>0.1371 | 0.1300<br>0.1304 |

**Table 3.** Dimensionless frequency $\beta^* = \omega h\sqrt{\rho_c / E_c}$ for SSSS FG square plate $(\eta = 2)$

| $\tau$ | $n$ | | | | | |
|---|---|---|---|---|---|---|
| | 0 | 0.5 | 1 | 2 | 5 | 10 |
| 0.05 | 0.0093 | 0.0079 | 0.0071 | 0.0064 | 0.0061 | 0.0059 |
| 0.1 | 0.0365 | 0.0310 | 0.0279 | 0.0254 | 0.0240 | 0.0232 |
| 0.2 | 0.1376 | 0.1173 | 0.1059 | 0.0961 | 0.0901 | 0.0867 |

**Table 4.** Dimensionless frequency $\beta^* = \omega h\sqrt{\rho_c / E_c}$ for SCSS FG square plate

| $\tau$ | $n$ | | | | | |
|---|---|---|---|---|---|---|
| | 0 | 0.5 | 1 | 2 | 5 | 10 |
| 0.05 | 0.0176 | 0.0150 | 0.0135 | 0.0123 | 0.0116 | 0.0112 |
| 0.1 | 0.0678 | 0.0576 | 0.0520 | 0.0473 | 0.0445 | 0.0428 |
| 0.2 | 0.2385 | 0.2048 | 0.1854 | 0.1680 | 0.1557 | 0.1486 |

**Table 5.** Dimensionless frequency $\beta^* = \omega h\sqrt{\rho_c / E_c}$ for SCSC FG square plate

| $\tau$ | $n$ | | | | | |
|---|---|---|---|---|---|---|
| | 0 | 0.5 | 1 | 2 | 5 | 10 |
| 0.05 | 0.0214 | 0.0182 | 0.0164 | 0.0149 | 0.0141 | 0.0136 |
| 0.1 | 0.0807 | 0.0688 | 0.0622 | 0.0565 | 0.0529 | 0.0508 |
| 0.2 | 0.2707 | 0.2336 | 0.2122 | 0.1921 | 0.1765 | 0.1675 |

### 7.2 Study on wave power reflection in FG plates

The power carried in propagating wave is proportional to the square of the wave amplitude. Therefore, the power reflected per unit incident power can be calculated by the square of the reflection coefficients $|r(i,j)|^2$ [25]. So, the reflected power can be calculated at the boundaries. The relation between positive and negative travelling waves with the reflection matrix $r$ could be defined as follow:

$$r(1,1)a_1^- + r(1,2)a_2^- + r(1,3)a_3^- = a_1^+ \tag{43a}$$

$$r(2,1)a_1^- + r(2,2)a_2^- + r(2,3)a_3^- = a_2^+ \tag{43b}$$

$$r(3,1)a_1^- + r(3,2)a_2^- + r(3,3)a_3^- = a_3^+ \tag{43c}$$

Therefore, $r(i,j)$ represents the reflection contribution of the j-th incident wave in the i-th reflected wave. Two types of waves are defined here: propagating wave and attenuating wave. If $\mu_1$ is real, the first wave is the propagating kind and if it is imaginary, it is attenuating one. Moreover, if $\mu_2$ and $\mu_3$ are real, the type of second and third wave is attenuating, and if they are imaginary, the wave type is propagating.

For the simply supported boundary condition, the reflection coefficients are constant. But for the clamped boundary condition, the situation is different. Figures 4-12 show the reflection matrix coefficients chart in terms of frequency for different values of power law index and clamped boundary condition. Here, the $\tau$ value equals to 0.2. As is clear, the curve has jumps or sharp drops at three points and these points are cut off frequencies. The frequency range is divided into four section. The first range is frequency values less than the first cut off frequency. The second range is frequency values between the first and second cut off frequency. The third range is frequency values between the second and third cut off frequency and the fourth range is frequency values more than the third cut off frequency. According to Figs. 4-12, it is observed that by increasing the power law index, the first cut off frequency increases and then decreases. Besides, by increasing the power law index, the second and third cut off frequencies decrease and then increase. The changing process of cut off frequency values due to the increase of power law index leads to defining the first critical power law index and the second critical power law index and here, they are specified as $n_{c1}$ and $n_{c2}$. In the first frequency range, by increasing the power law index, the coefficients $r(3,1)$, $r(3,2)$, and $r(3,3)$ increase until they reach to $n_{c2}$ and then decrease. This means that by increasing the power law index to $n_{c2}$, the power of reflected wave with $\mu_3$ wave number increases and by increasing the power law index for more than $n_{c2}$, the waves power with $\mu_3$ wave number decreases.

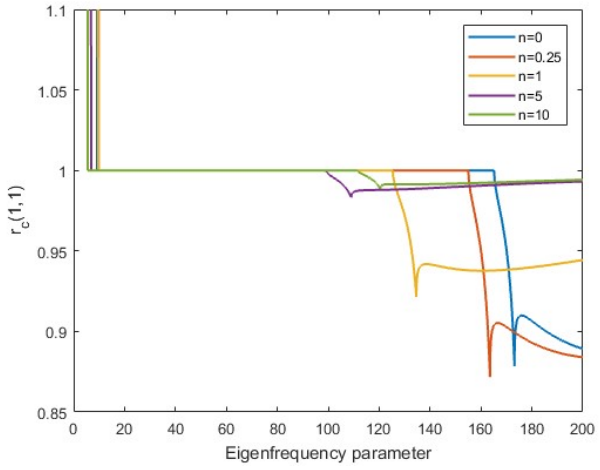


**Fig. 4.** Variation of $r_c(1,1)$ with respect to eigenfrequency parameter

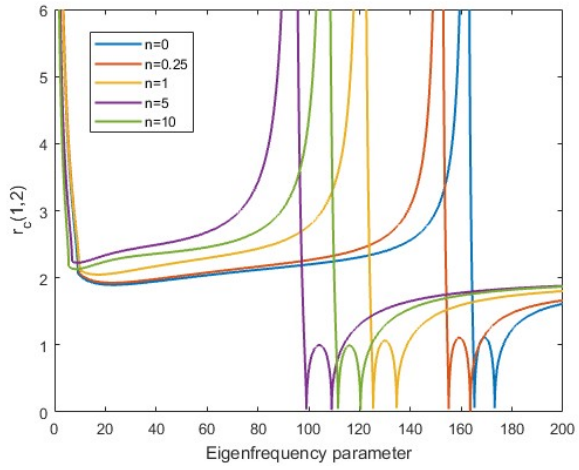


**Fig. 5.** Variation of $r_c(1,2)$ with respect to eigenfrequency parameter

In the second frequency range, the values of second cut off frequency are decreased by increasing the power law index until

it reaches to $n_{c2}$ and then increase. The value of $r(1,1)$ coefficient is constant for each power law index and equals to the unit. Therefore, if the wave with $\mu_1$ wave number encounters to a clamped boundary condition, the power of reflected wave with $\mu_1$ wave number is always equal to the initial wave. In addition, by increasing the frequency value, $r(2,2)$ and $r(3,3)$ increase and then decrease until they reach to the unit value. In other words, if the wave with $\mu_2$ and $\mu_3$ wave number encounters to a clamped boundary condition in the second cut off frequency, the power of reflected wave with $\mu_2$ and $\mu_3$ wave number is equal to the initial wave, respectively. In this frequency range, all coefficients of reflectance matrix except

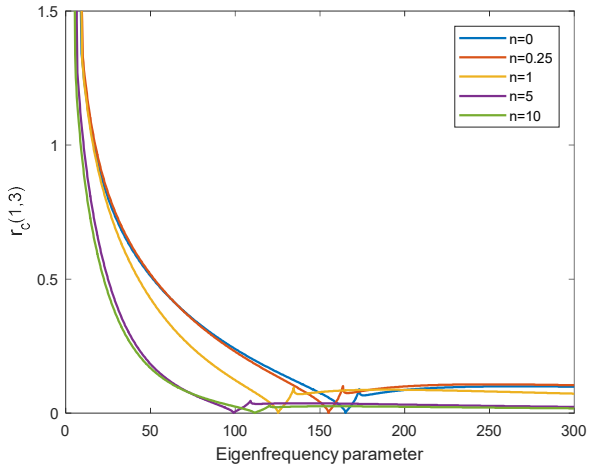


**Fig. 6.** Variation of $r_c(1,3)$ with respect to eigenfrequency parameter

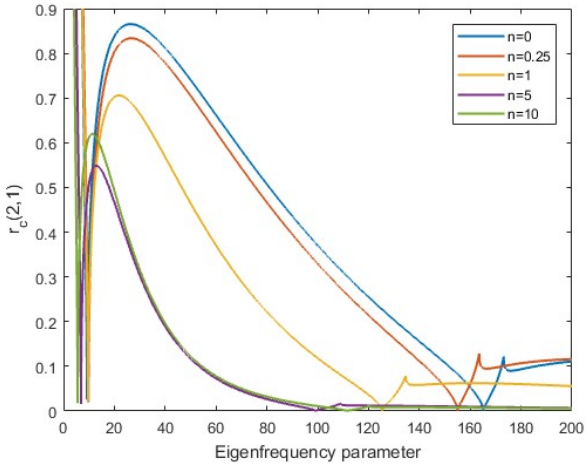


**Fig. 7.** Variation of $r_c(2,1)$ with respect to eigenfrequency parameter

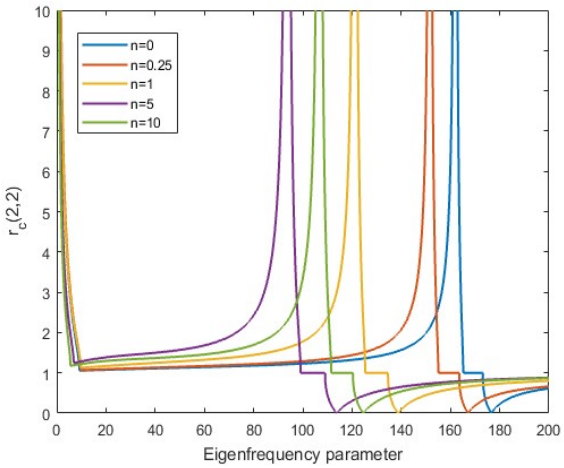


**Fig. 8.** Variation of $r_c(2,2)$ with respect to eigenfrequency parameter

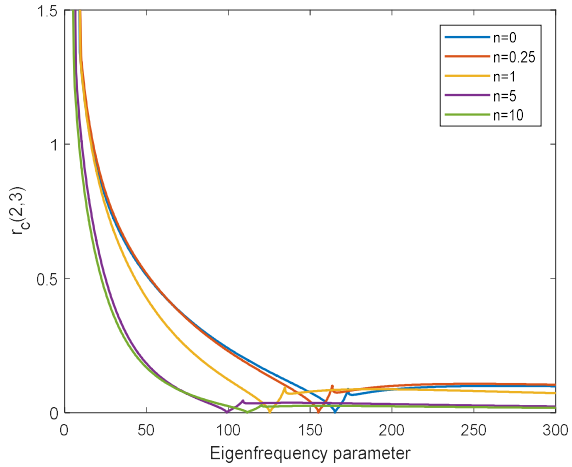


**Fig. 9.** Variation of $r_c(2,3)$ with respect to eigenfrequency parameter

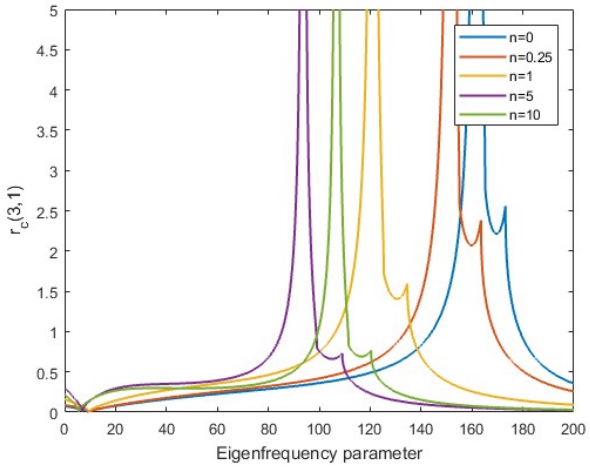


**Fig. 10.** Variation of $r_c(3,1)$ with respect to eigenfrequency parameter

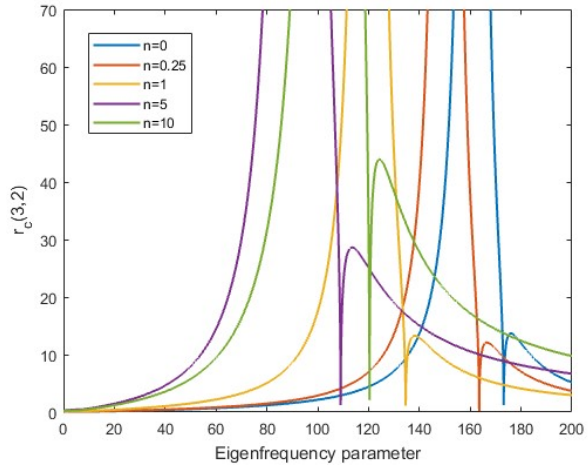


**Fig. 11.** Variation of $r_c(3,2)$ with respect to eigenfrequency parameter

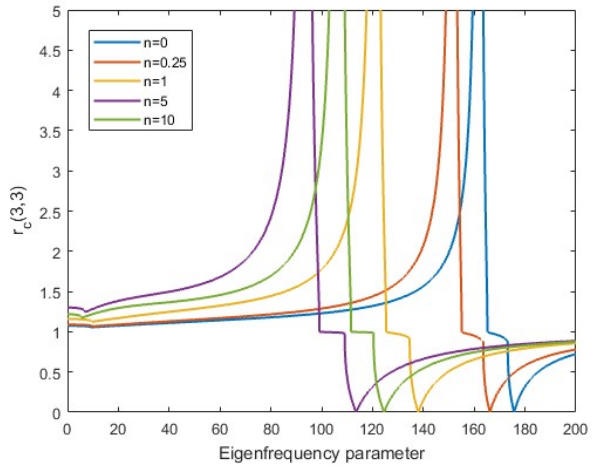


**Fig. 12.** Variation of $r_c(3,3)$ with respect to eigenfrequency parameter

for $r(1,1)$, $r(2,1)$, $r(1,3)$, and $r(2,3)$ by increasing the power law index to $n_{c2}$ increase and then decrease. In this frequency range, the value of $r(1,3)$ and $r(2,3)$ coefficients varies in two ways. Until half the second frequency range, these coefficients increase with increasing the power law index until they reach to $n_{c1}$ and then decrease. Then, for the rest of the second frequency range, these coefficients decrease with increasing the power law index until they reach to $n_{c2}$ and then increase. The $r(2,1)$ coefficient value decrease with increasing the power law index until they reach to $n_{c2}$ and then increase. Moreover, the $r(1,1)$ value is constant and independent of the power law index.

In the third frequency range, the values of the third cut off frequency are reduced by increasing the power law index until it reaches the value of $n_{c2}$ and then increases. In this range, the values of coefficients of $r(2,2)$ and $r(3,3)$ for all values of the FGM parameter are approximately constant and equal to one. Moreover, the values of $r(1,1)$ and $r(3,2)$ reduce with increasing frequency and the values of $r(1,3)$ ،$r(2,1)$ ،$r(2,3)$ and $r(3,1)$ increase by increasing the frequency. Also, the value of $r(1,2)$ increases until it reaches the maximum value, and then decreases until reaching the value of zero. The value of coefficients $r(1,1)$ and $r(3,2)$ decreases until it reaches $n_{c1}$ with increasing the power law index and then increases. The value of the coefficient $r(3,1)$ decreases until it reaches $n_{c2}$ with increasing the power law index meter and then increases. Besides, the rest of the reflection matrix coefficients increases until it reaches $n_{c1}$ with increasing the power law index and then decreases.

In the fourth frequency range, the values of the coefficients $r(1,1)$ ,$r(2,2)$, and $r(3,3)$ converge to the unit value. This means that, when a wave with a wave number of $\mu_1$, $\mu_2$, and $\mu_3$ encounters a clamped boundary condition at a high frequency range, the reflection wave power with the wave number of $\mu_1$ ،$\mu_2$ , and $\mu_3$ res $r(1,2)$ in the high frequency range approaches to 2. That is, in the high frequency range, if the wave with a wave number of $\mu_2$ encounters a clamped boundary condition, the wave power reflected with the wave number of $\mu_2$ will be four times greater. The rest of the reflection matrix coefficients approach zero at a high frequency range. In this frequency range, the value of coefficients $r(1,1)$ and $r(3,2)$ with increasing the power law index decreases by the $n_{c1}$ and then increase. The value of coefficients $r(1,3)$ and $r(2,3)$ increase up to $n_{c1}$ by increasing power law index and then decrease. The value of the coefficient $r(3,1)$ decreases until it reaches $n_{c2}$ with increasing the power law index and then increases. Also, the other reflection matrix coefficients increase up to $n_{c1}$ then by increasing the power law index decrease.

## 8. Conclusion

This paper presents the free vibration analysis of the rectangular Mindlin plates using wave propagation method. Dimensionless natural frequencies of the plate are compared with the available literature and excellent agreement is observed. Also, for the first time, the effect of power law index on wave power reflection was studied. It was observed that by increasing the FGM parameter, the first cut off frequency increases and then decreases. Also, by increasing the FGM Parameter, the second and third cut off frequencies decrease and then increase. The changing process of cut off frequency values due to the increase of FGM parameter leads to defining the first critical FGM parameter and the second critical FGM parameter.

## Conflict of Interest

The authors declare no conflict of interest.

## References

[1] Zhao, X., Y. Lee, and K.M. Liew, Free vibration analysis of functionally graded plates using the element-free kp-Ritz method. *Journal of sound and Vibration*, 319(3-5), 2009, 918-939.

[2] El Meiche, N., Tounsi, A., Ziane, N., Mechab, I., Adda.Bediaa, E.A., A new hyperbolic shear deformation theory for buckling and vibration of functionally graded sandwich plate. *International Journal of Mechanical Sciences*, 53(4), 2011, 237-247.

[3] Hosseini-Hashemi, S., Rokni Damavandi Taher, H., Akhavana, H., Omidia, M., Free vibration of functionally graded rectangular plates using first-order shear deformation plate theory. *Applied Mathematical Modelling*, 34(5), 2010, 1276-1291.

[4] Akbaş, Ş.D., Free vibration characteristics of edge cracked functionally graded beams by using finite element method. *International Journal of Engineering Trends and Technology*, 4(10), 2013, 4590-4597.

[5] Thai, H.-T., Vo, T.P., A new sinusoidal shear deformation theory for bending, buckling, and vibration of functionally graded plates. *Applied mathematical modelling*, 37(5), 2013, 3269-3281.

[6] Mahi, A., Tounsi, A., A new hyperbolic shear deformation theory for bending and free vibration analysis of isotropic, functionally graded, sandwich and laminated composite plates. *Applied Mathematical Modelling*, 39(9), 2015, 2489-2508.

[7] Akbaş, Ş.D., Free vibration and bending of functionally graded beams resting on elastic foundation. *Research on Engineering Structures and Materials*, 1(1), 2015, 25-37.

[8] Bennoun, M., Houari, M.S.A., Tounsi, A., A novel five-variable refined plate theory for vibration analysis of functionally graded sandwich plates. *Mechanics of Advanced Materials and Structures*, 23(4), 2016, 423-431.

[9] Zhang, L., Lei, Z., Liew, K., Free vibration analysis of functionally graded carbon nanotube-reinforced composite triangular plates using the FSDT and element-free IMLS-Ritz method. *Composite Structures*, 120, 2015, 189-199.

[10] Khorshidi, K., Asgari, T., Fallah, A., Free vibrations analysis of functionally graded rectangular nano-plates based on nonlocal exponential shear deformation theory. *Mechanics of Advanced Composite Structures*, 2(2), 2015, 79-93.

[11] Bellifa, H., BenrahouL, K.H., Hadji, L., Houari, M.S.A., Tounsi, A., Bending and free vibration analysis of functionally graded plates using a simple shear deformation theory and the concept the neutral surface position. *Journal of the Brazilian Society of Mechanical Sciences and Engineering*, 38(1), 2016, 265-275.

[12] Pradhan, K., Chakraverty, S., Free vibration of functionally graded thin elliptic plates with various edge supports. *Structural Engineering and Mechanics*, 53(2), 2015, 337-354.

[13] Houari, M.S.A., et al., A new simple three-unknown sinusoidal shear deformation theory for functionally graded plates. *Steel and Composite Structures*, 22(2), 2016, 257-276.

[14] Bounouara, F., et al., A nonlocal zeroth-order shear deformation theory for free vibration of functionally graded nanoscale plates resting on elastic foundation. *Steel and Composite Structures*, 20(2), 2016, 227-249.

[15] Abdelbari, S., et al., An efficient and simple shear deformation theory for free vibration of functionally graded rectangular plates on Winkler-Pasternak elastic foundations. *Wind and Structures*, 22(3), 2016, 329-348.

[16] Akbaş, Ş.D., Vibration and static analysis of functionally graded porous plates. *Journal of Applied and Computational Mechanics*, 3(3), 2017, 199-207.

[17] Bessaim, A., et al., Buckling analysis of embedded nanosize FG beams based on a refined hyperbolic shear deformation theory. *Journal of Applied and Computational Mechanics*, 4(3), 2018, 140-146.

[18] Fouda, N., T. El-midany, and A. Sadoun, Bending, buckling and vibration of a functionally graded porous beam using finite elements. *Journal of Applied and Computational Mechanics*, 3(4), 2017, 274-282.

[19] Song, M., S. Kitipornchai, and J. Yang, Free and forced vibrations of functionally graded polymer composite plates reinforced with graphene nanoplatelets. *Composite Structures*, 159, 2017, 579-588.

[20] Akbaş, Ş.D., Stability of a Non-Homogenous Porous Plate by Using Generalized Differantial Quadrature Method. *International Journal of Engineering & Applied Sciences*, 9(2), 2017, 147-155.

[21] Akbaş, Ş.D., Free vibration of edge cracked functionally graded microscale beams based on the modified couple stress theory. *International Journal of Structural Stability and Dynamics*, 17(3), 2017, 1750033.

[22] Akbaş, Ş.D., Forced vibration analysis of functionally graded nanobeams. *International Journal of Applied Mechanics*, 9(7), 2017, 1750100.

[23] Akbaş, Ş.D., Thermal Effects on the Vibration of Functionally Graded Deep Beams with Porosity. *International Journal of Applied Mechanics*, 9(5), 2017, 1750076.

[24] Akbaş, Ş.D., Forced vibration analysis of functionally graded porous deep beams. *Composite Structures*, 186, 2018, 293-302.

[25] Mace, B., Wave reflection and transmission in beams. *Journal of Sound and Vibration*, 97(2), 1984, 237-246.

[26] Mei, C. Mace, B., Wave reflection and transmission in Timoshenko beams and wave analysis of Timoshenko beam structures. *Journal of Vibration and Acoustics*, 127(4), 2005, 382-394.

[27] Bahrami, M.N., Arani, M.K., Saleh, N.R., Modified wave approach for calculation of natural frequencies and mode shapes

in arbitrary non-uniform beams. *Scientia Iranica*, 18(5), 2011, 1088-1094.

[28] Bahrami, A., Ilkhani, M.R., Bahrami, M.N., Wave propagation technique for free vibration analysis of annular circular and sectorial membranes. *Journal of Vibration and Control*, 21(9), 2015, 1866-1872.

[29] Bahrami, A., Teimourian, A. Nonlocal scale effects on buckling, vibration and wave reflection in nanobeams via wave propagation approach. *Composite Structures*, 134, 2015, 1061-1075.

[30] Ilkhani, M., Bahrami, A., Hosseini-Hashemi, S., Free vibrations of thin rectangular nano-plates using wave propagation approach. *Applied Mathematical Modelling*, 40(2), 2016, 1287-1299.

[31] Bahrami, A., Teimourian, A., Study on the effect of small scale on the wave reflection in carbon nanotubes using nonlocal Timoshenko beam theory and wave propagation approach. *Composites Part B: Engineering*, 91, 2016, 492-504.

[32] Bahrami, A., Teimourian, A., Free vibration analysis of composite, circular annular membranes using wave propagation approach. *Applied Mathematical Modelling*, 39(16), 2015, 4781-4796.

[33] Bahrami, A., Teimourian, A., Study on vibration, wave reflection and transmission in composite rectangular membranes using wave propagation approach. *Meccanica*, 52(1-2), 2017, 231-249.

[34] Bahrami, A., Teimourian, A., Small scale effect on vibration and wave power reflection in circular annular nanoplates. *Composites Part B: Engineering*, 109, 2017, 214-226.

[35] Bahrami, A., Free vibration, wave power transmission and reflection in multi-cracked nanorods. *Composites Part B: Engineering*, 127, 2017, 53-62.

[36] Bahrami, A., A wave-based computational method for free vibration, wave power transmission and reflection in multi-cracked nanobeams. *Composites Part B: Engineering*, 120, 2017, 168-181.

[37] Akbaş, Ş.D., Wave propagation analysis of edge cracked circular beams under impact force. *PloS One*, 9(6), 2014, 100496.

[38] Akbas, S.D., Wave propagation of a functionally graded beam in thermal environments. *Steel and Composite Structures*, 19(6), 2015, 1421-1447.

[39] Akbaş, Ş.D., Wave propagation in edge cracked functionally graded beams under impact force. *Journal of Vibration and Control*, 22(10), 2016, 2443-2457.

[40] Shen, H.-S., Nonlinear bending response of functionally graded plates subjected to transverse loads and in thermal environments. *International Journal of Mechanical Sciences*, 44(3), 2002, 561-584.